Research Article | Vol. 26, No. 12 | 11 Jun 2018 | OPTICS EXPRESS 15935
Optics EXPRESS

Graphene-based hybrid plasmonic waveguide for highly efficient broadband mid-infrared propagation and modulation

LONGFANG YE,[1,2,*] KEHAN SUI,[1] YANHUI LIU,[1] MIAO ZHANG,[1] AND QING HUO LIU[3]

[1]*Institute of Electromagnetics and Acoustics, and Department of Electronic Science, Xiamen University, Xiamen 361005, China*
[2]*Shenzhen Research Institute of Xiamen University, Shenzhen 518057, China*
[3]*Department of Electrical and Computer Engineering, Duke University, Durham 27708, USA*
[*]*lfye@xmu.edu.cn*

Abstract: In this paper, a graphene-based hybrid plasmonic waveguide is proposed for highly efficient broadband surface plasmon polariton (SPP) propagation and modulation at mid-infrared (mid-IR) spectrum. The hybrid plasmonic waveguide is composed of a monolayer graphene sheet in the center, a polysilicon gating layer, and two inner dielectric buffer layers and two outer parabolic-ridged silicon substrates symmetrically placed on both sides of the graphene. Owing to the unique parabolic-ridged waveguide structure, the light-graphene interaction and subwavelength SPPs confinement of the fundamental SPP mode for the hybrid waveguide can be significantly increased. Under the graphene chemical potential of 1.0 eV, the proposed waveguide can achieve outstanding SPP propagation performance with long propagation length of 12.1-16.7 μm and small normalized mode area of ~10^{-4} in the frequency range of 10-20 THz, exhibiting more than one order smaller in the normalized mode area while remaining the propagation length almost the same level with respect to the hybrid plasmonic waveguide without parabolic ridges. By tuning the graphene chemical potential from 0.1 to 1.0 eV, we demonstrate the waveguide has a modulation depth greater than 51% for the frequency ranging from 10 to 20 THz and reaches a maximum of nearly 100% at the frequency higher than 18 THz. Benefitting from the excellent broadband mid-IR propagation and modulation performance, the graphene-based hybrid plasmonic waveguide may open up a new way for various mid-IR waveguides, modulators, interconnects and optoelectronic devices.

OCIS codes: (040.2235) Far infrared or terahertz; (240.6680) Surface plasmons; (130.2790) Guided waves; (230.7370) Waveguides; (230.4110) Modulators; (130.3120) Integrated optics devices.

References and links

1. R. Soref, "Mid-infrared photonics in silicon and germanium," Nat. Photonics **4**(8), 495–497 (2010).
2. M. Schnell, P. Alonso-Gonzalez, L. Arzubiaga, F. Casanova, L. E. Hueso, A. Chuvilin, and R. Hillenbrand, "Nanofocusing of mid-infrared energy with tapered transmission lines," Nat. Photonics **5**(5), 283–287 (2011).
3. D. K. Gramotnev and S. I. Bozhevolnyi, "Plasmonics beyond the diffraction limit," Nat. Photonics **4**(2), 83–91 (2010).
4. E. Ozbay, "Plasmonics: Merging photonics and electronics at nanoscale dimensions," Science **311**(5758), 189–193 (2006).
5. C. Yang, Q. Wu, J. Xu, K. A. Nelson, and C. A. Werley, "Experimental and theoretical analysis of THz-frequency, direction-dependent, phonon polariton modes in a subwavelength, anisotropic slab waveguide," Opt. Express **18**(25), 26351–26364 (2010).
6. N. Ranjkesh, M. Basha, A. Taeb, A. Zandieh, S. Gigoyan, and S. Safavi-Naeini, "Silicon-on-glass dielectric waveguide—Part I: For millimeter-wave integrated circuits," IEEE Trans. THz Sci. Technol. **5**(2), 268–279 (2015).
7. T. S. Saini, A. Kumar, and R. K. Sinha, "Broadband Mid-Infrared Supercontinuum Spectra Spanning 2-15 μm Using As2Se3 Chalcogenide Glass Triangular-Core Graded-Index Photonic Crystal Fiber," J. Lightwave Technol. **33**(18), 3914–3920 (2015).
8. R. Zia, J. A. Schuller, A. Chandran, and M. L. Brongersma, "Plasmonics: the next chip-scale technology,"

#330594 https://doi.org/10.1364/OE.26.015935
Journal © 2018 Received 30 Apr 2018; revised 1 Jun 2018; accepted 2 Jun 2018; published 8 Jun 2018

Optics EXPRESS

Mater. Today **9**(7–8), 20–27 (2006).
9. C. L. Smith, N. Stenger, A. Kristensen, N. A. Mortensen, and S. I. Bozhevolnyi, "Gap and channeled plasmons in tapered grooves: a review," Nanoscale **7**(21), 9355–9386 (2015).
10. R. F. Oulton, V. J. Sorger, D. A. Genov, D. F. P. Pile, and X. Zhang, "A hybrid plasmonic waveguide for subwavelength confinement and long-range propagation," Nat. Photonics **2**(8), 496–500 (2008).
11. Z. Zhang and J. Wang, "Long-range hybrid wedge plasmonic waveguide," Sci. Rep. **4**(1), 6870 (2014).
12. Y. Gao, G. Ren, B. Zhu, J. Wang, and S. Jian, "Single-mode graphene-coated nanowire plasmonic waveguide," Opt. Lett. **39**(20), 5909–5912 (2014).
13. J. B. Pendry, L. Martín-Moreno, and F. J. Garcia-Vidal, "Mimicking surface plasmons with structured surfaces," Science **305**(5685), 847–848 (2004).
14. X. Shen, T. J. Cui, D. Martin-Cano, and F. J. Garcia-Vidal, "Conformal surface plasmons propagating on ultrathin and flexible films," Proc. Natl. Acad. Sci. U.S.A. **110**(1), 40–45 (2013).
15. A. K. Geim, "Graphene: status and prospects," Science **324**(5934), 1530–1534 (2009).
16. A. N. Grigorenko, M. Polini, and K. S. Novoselov, "Graphene plasmonics," Nat. Photonics **6**(11), 749–758 (2012).
17. T. Low and P. Avouris, "Graphene plasmonics for terahertz to mid-infrared applications," ACS Nano **8**(2), 1086–1101 (2014).
18. F. H. Koppens, D. E. Chang, and F. J. García de Abajo, "Graphene plasmonics: a platform for strong light-matter interactions," Nano Lett. **11**(8), 3370–3377 (2011).
19. Z. Fei, A. S. Rodin, G. O. Andreev, W. Bao, A. S. McLeod, M. Wagner, L. M. Zhang, Z. Zhao, M. Thiemens, G. Dominguez, M. M. Fogler, A. H. Castro Neto, C. N. Lau, F. Keilmann, and D. N. Basov, "Gate-tuning of graphene plasmons revealed by infrared nano-imaging," Nature **487**(7405), 82–85 (2012).
20. V. W. Brar, M. S. Jang, M. Sherrott, J. J. Lopez, and H. A. Atwater, "Highly confined tunable mid-infrared plasmonics in graphene nanoresonators," Nano Lett. **13**(6), 2541–2547 (2013).
21. A. Vakil and N. Engheta, "Transformation optics using graphene," Science **332**(6035), 1291–1294 (2011).
22. D. Rodrigo, O. Limaj, D. Janner, D. Etezadi, F. J. García de Abajo, V. Pruneri, and H. Altug, "Mid-infrared plasmonic biosensing with graphene," Science **349**(6244), 165–168 (2015).
23. L. Ye, Y. Chen, G. Cai, N. Liu, J. Zhu, Z. Song, and Q. H. Liu, "Broadband absorber with periodically sinusoidally-patterned graphene layer in terahertz range," Opt. Express **25**(10), 11223–11232 (2017).
24. L. Luo, K. Wang, C. Ge, K. Guo, F. Shen, Z. Yin, and Z. Guo, "Actively controllable terahertz switches with graphene-based nongroove gratings," Photon. Res. **5**(6), 604–611 (2017).
25. M. Liu, X. Yin, E. Ulin-Avila, B. Geng, T. Zentgraf, L. Ju, F. Wang, and X. Zhang, "A graphene-based broadband optical modulator," Nature **474**(7349), 64–67 (2011).
26. M. Liu, X. Yin, and X. Zhang, "Double-layer graphene optical modulator," Nano Lett. **12**(3), 1482–1485 (2012).
27. M. Hajati and Y. Hajati, "High-performance and low-loss plasmon waveguiding in graphene-coated nanowire with substrate," J. Opt. Soc. Am. B **33**(12), 2560–2565 (2016).
28. W. Luo, W. Cai, Y. Xiang, L. Wang, M. Ren, X. Zhang, and J. Xu, "Flexible modulation of plasmon-induced transparency in a strongly coupled graphene grating-sheet system," Opt. Express **24**(6), 5784–5793 (2016).
29. S. X. Xia, X. Zhai, L. L. Wang, B. Sun, J. Q. Liu, and S. C. Wen, "Dynamically tunable plasmonically induced transparency in sinusoidally curved and planar graphene layers," Opt. Express **24**(16), 17886–17899 (2016).
30. P. A. D. Gonçalves, E. J. C. Dias, S. Xiao, M. I. Vasilevskiy, N. A. Mortensen, and N. M. R. Peres, "Graphene plasmons in triangular wedges and grooves," ACS Photonics **3**(11), 2176–2183 (2016).
31. Z. Vafapour, Y. Hajati, M. Hajati, and H. Ghahraloud, "Graphene-based mid-infrared biosensor," J. Opt. Soc. Am. B **34**(12), 2586–2592 (2017).
32. M. Hajati and Y. Hajati, "Dynamic tuning of mid-infrared plasmons in graphene–buffer–SiO_2–Si nanostructures," J. Opt. Soc. Am. B **33**(6), 1303–1310 (2016).
33. Y. Zhang, S. Qiao, S. Liang, Z. Wu, Z. Yang, Z. Feng, H. Sun, Y. Zhou, L. Sun, Z. Chen, X. Zou, B. Zhang, J. Hu, S. Li, Q. Chen, L. Li, G. Xu, Y. Zhao, and S. Liu, "Gbps terahertz external modulator based on a composite metamaterial with a double-channel heterostructure," Nano Lett. **15**(5), 3501–3506 (2015).
34. G. Liang, X. Hu, X. Yu, Y. Shen, L. H. Li, A. G. Davies, E. H. Linfield, H. K. Liang, Y. Zhang, S. F. Yu, and Q. J. Wang, "Integrated terahertz graphene modulator with 100% modulation depth," ACS Photonics **2**(11), 1559–1566 (2015).
35. Y. Wang, T. Li, and S. Zhu, "Graphene-based plasmonic modulator on a groove-structured metasurface," Opt. Lett. **42**(12), 2247–2250 (2017).
36. J. Gosciniak and D. T. Tan, "Theoretical investigation of graphene-based photonic modulators," Sci. Rep. **3**(1), 1897 (2013).
37. F. A. Vallejo and L. M. Hayden, "Design of ultra-broadband terahertz polymer waveguide emitters for telecom wavelengths using coupled mode theory," Opt. Express **21**(5), 5842–5858 (2013).
38. P. D. Cunningham, N. N. Valdes, F. A. Vallejo, L. M. Hayden, B. Polishak, X. H. Zhou, and R. J. Twieg, "Broadband terahertz characterization of the refractive index and absorption of some important polymeric and organic electro-optic materials," J. Appl. Phys. **109**(4), 043505 (2011).
39. M. Faraji, M. K. Moravvej-Farshi, and L. Yousefi, "Tunable THz perfect absorber using graphene-based metamaterials," Opt. Commun. **355**, 352–355 (2015).
40. J. S. Gómez-Díaz, M. Esquius-Morote, and J. Perruisseau-Carrier, "Plane wave excitation-detection of non-resonant plasmons along finite-width graphene strips," Opt. Express **21**(21), 24856–24872 (2013).

Optics EXPRESS

41. Y. Zhao, E. Berenschot, H. Jansen, N. Tas, J. Huskens, and M. Elwenspoek, "Sub-10 nm silicon ridge nanofabrication by advanced edge lithography for NIL applications," Microelectron. Eng. **86**(4–6), 832–835 (2009).
42. H. D. Nayeri, R. Asadi, and M. Malekmohammad, "Fabrication of optical ridge waveguide in lithium niobate by argon sputtering and titanium self-alignment in-diffusion," J. Nanophotonics **10**(3), 036016 (2016).
43. Y. Lee, S. Bae, H. Jang, S. Jang, S. E. Zhu, S. H. Sim, Y. I. Song, B. H. Hong, and J. H. Ahn, "Wafer-scale synthesis and transfer of graphene films," Nano Lett. **10**(2), 490–493 (2010).
44. Q. Q. Zhuo, Q. Wang, Y. P. Zhang, D. Zhang, Q. L. Li, C. H. Gao, Y. Q. Sun, L. Ding, Q. J. Sun, S. D. Wang, J. Zhong, X. H. Sun, and S. T. Lee, "Transfer-free synthesis of doped and patterned graphene films," ACS Nano **9**(1), 594–601 (2015).
45. M. S. Kwon, "Discussion of the epsilon-near-zero effect of graphene in a horizontal slot waveguide," IEEE Photonics J. **6**(3), 1–9 (2014).
46. J. Zhu, J. Cheng, L. Zhang, and Q. H. Liu, "Modeling of 2D graphene material for plasmonic hybrid waveguide with enhanced near-infrared modulation," Mater. Lett. **186**, 53–56 (2017).
47. R. Yu, V. Pruneri, and F. J. García de Abajo, "Resonant visible light modulation with graphene," ACS Photonics **2**(4), 550–558 (2015).
48. G. W. Hanson, "Dyadic Green's functions and guided surface waves for a surface conductivity model of graphene," J. Appl. Phys. **103**(6), 064302 (2008).
49. G. W. Hanson, "Dyadic Green's functions for an anisotropic, non-local model of biased graphene," IEEE Trans. Antenn. Propag. **56**(3), 747–757 (2008).
50. K. I. Bolotin, K. J. Sikes, Z. Jiang, M. Klima, G. Fudenberg, J. Hone, and H. L. Stormer, "Ultrahigh electron mobility in suspended graphene," Solid State Commun. **146**(9–10), 351–355 (2008).
51. W. Gao, J. Shu, C. Qiu, and Q. Xu, "Excitation of plasmonic waves in graphene by guided-mode resonances," ACS Nano **6**(9), 7806–7813 (2012).
52. C. R. Dean, A. F. Young, I. Meric, C. Lee, L. Wang, S. Sorgenfrei, K. Watanabe, T. Taniguchi, P. Kim, K. L. Shepard, and J. Hone, "Boron nitride substrates for high-quality graphene electronics," Nat. Nanotechnol. **5**(10), 722–726 (2010).
53. Q. Zhang, X. Li, M. M. Hossain, Y. Xue, J. Zhang, J. Song, J. Liu, M. D. Turner, S. Fan, Q. Bao, and M. Gu, "Graphene surface plasmons at the near-infrared optical regime," Sci. Rep. **4**(1), 6559 (2014).
54. W. Xu, Z. H. Zhu, K. Liu, J. F. Zhang, X. D. Yuan, Q. S. Lu, and S. Q. Qin, "Toward integrated electrically controllable directional coupling based on dielectric loaded graphene plasmonic waveguide," Opt. Lett. **40**(7), 1603–1606 (2015).
55. X. Hu and J. Wang, "Design of graphene-based polarization-insensitive optical modulator," Nanophotonics **7**(3), 651–658 (2018).

1. Introduction

Mid-infrared radiation, with the wavelength ranging from 3 μm to 30 μm, has attracted increasing attention in recent years, owing to its extensive exciting applications in imaging, sensing, spectroscopy, and communications [1, 2]. Waveguides are one variety of the most fundamental components of the optical integrated circuits and systems to transmit electromagnetic waves. It would be greatly promising to develop new mid-IR waveguides with superior properties of low loss, deep confinement, and flexible tunability. Surface plasmon polaritons (SPPs) are surface electromagnetic (EM) waves that propagate along a metal-air/dielectric interface from visible to near-infrared spectral region [3, 4]. Compared to the dielectric-based waveguides, e.g., slab waveguides [5], silicon-on-glass waveguides [6], and photonic crystal fibers [7], metal-based SPP waveguides are capable of guiding light with subwavelength confinement beyond the diffraction limit, demonstrating great potential in highly integrated optical circuits at the chip level [8]. In recent years, various metal-based SPPs waveguides have been theoretically and experimentally studied, such as metal gap, channeled, and wedged plasmonic waveguides [9]. However, these waveguides usually support the short- or long-range SPPs suffering from a trade-off between mode confinement and propagation length. In order to further improve the SPP propagation length, a diverse set of metal-based hybrid plasmonic waveguides have been investigated [10, 11]. It is found that the SPPs supported by these types of waveguides can achieve long-range propagation of $\sim 10^{1}$-10^{5} μm with the normalized mode area of $\sim 10^{-3}$-10^{0} at the wavelength of 1.55 μm. However, directly extending this waveguiding scheme to the mid-IR region will lead to a significant deterioration in the subwavelength confinement, making it unsuitable for compact integration [12]. In the other hand, based on the concept of spoof SPPs, many subwavelength textured metal surface structures have been proposed to enhance the field confinement at

Optics EXPRESS

microwave or lower terahertz frequencies [13, 14]. But it still remains a challenge to extend the spoof SPP properties to mid-IR owing to the difficulty in achieving nanoscale dimensions [2]. Furthermore, by employing noble metal and normal dielectric materials without electric or magnetic tunability, all abovementioned plasmonic waveguides suffer from the inherent drawback of not adjustable once the structures are fixed after fabrication.

Graphene, a single layer of carbon atoms, has attracted great interest owing to its unique mechanical, electrical, and optical properties [15, 16]. Because of supporting surface plasmons in the terahertz and infrared ranges, graphene is considered as one of the most promising SPP materials superior to noble metals with much stronger mode confinement, relatively small propagation loss, especially with a significant advantage of being actively tunable via chemical doping or electrostatic doping [17, 18]. The graphene-based plasmonic waveguide expresses deep subwavelength confinement with the wavelength two orders smaller than that in free space [19–21]. The actively tunable properties, via electrostatic gating without changing the device structures, enable the graphene with a wide potential application in various tunable terahertz and infrared devices. Recently, many graphene-based tunable plasmonic devices including waveguides, modulators, switches, absorbers, and biosensors have been studied [21–32]. For example, Liu et al. first experimentally demonstrated single- and double-layer graphene optical waveguide modulator by integrating the graphene layer(s) on a Si substrate with the attenuation modulation of ~0.1-0.16 dB/μm [25, 26]. Subsequently, many efforts have been devoted to improving the waveguide modulation depth. Although there are some efficient spatial graphene modulators by integrating a composite metamaterial with modulation depth of up to 85% [33] and by incorporating a QCL cavity with modulation depth of up to 100% [34] under normal incidence have been achieved, the attenuation modulation (or modulation depth) of the graphene-based waveguide modulators is still low. Recently, a graphene-based modulator on a groove-structured metasurface has been proposed with an enhanced attenuation modulation of 0.47 dB/μm and a lower mode loss of 0.31 dB/μm [35]. By placing the graphene layers in position with the maximum of the electric field in the waveguide, a modulation depth of 5.75 dB/μm can be achieved [36]. Despite the recent progress, it still remains a significant challenge to develop novel graphene-based plasmonic waveguides for broadband mid-IR propagation and modulation with lower insertion loss and stronger subwavelength confinement, as well as ultra-high modulation depth in the mid-IR regime.

To address this issue, we propose a new graphene-based hybrid plasmonic waveguide for highly efficient broadband mid-IR SPP propagation and modulation. Special waveguide structure by integrating a single-layer graphene sheet between two sets of buffers and parabolic-ridged substrates is designed to increase light-graphene integration and SPP confinement on the graphene layer, and a gating layer is inserted below graphene to actively manipulate waveguide performance. To demonstrate the strong subwavelength confinement of the proposed waveguide, we first simulate and compare the fundamental SPP mode distributions, propagation length, and normalized mode area between the hybrid plasmonic waveguides with and without parabolic ridges. Then, the dependence of propagation properties of the first 5 SPP modes on the key geometric parameters of the parabolic ridges is studied. Under the chemical potential of 1.0 eV, the fundamental SPP mode with longer propagation length and smaller normalized mode is superior to other higher SPP modes in the mid-IR frequency range between 10 THz and 20 THz. Further, we demonstrate broadband mid-IR modulation properties of fundamental SPP mode of the proposed waveguide. By electrically tuning the graphene chemical potential, the waveguide provides an ultra-high SPP attenuation tuning capability over 136.6 dB/μm at 15 THz, which is so far the highest value to the best of our knowledge. In the broadband frequency range of 10-20 THz, the modulation depth greater than 51% is achieved, which approaches nearly 100% at the frequency higher than 18 THz. This study provides a new route to designing graphene-based hybrid plasmonic

Optics EXPRESS

waveguides for highly efficient broadband mid-IR propagation and modulation and may offer some interesting solutions for mid-IR interconnects and communications.

2. Design, simulation, and consideration

The schematic configuration of the proposed graphene-based hybrid plasmonic waveguide is displayed in Fig. 1, which is composed of two identical outer parabolic-ridged substrates and two identical inner buffer layers symmetrically placed on both sides of a monolayer graphene sheet in the center. The substrate layers are assumed to be silicon (Si) with the relative permittivity $\varepsilon_{Si} = 11.7$ and thickness $s = 600$ nm. The buffer layers are assumed to be Topas [37–39] with the relative permittivity $\varepsilon_{Topas} = 2.35$ and thickness $h = 600$ nm. The double silicon parabolic ridges, with their opening width and vertex-to-graphene separation as $W = 600$ nm and $T = 50$ nm, extend symmetrically into the Topas layers to enhance the light-graphene interaction and SPP confinement. By taking into account the feasibility of the gating scheme, a polysilicon film with the relative permittivity $\varepsilon_p = 3$ [40] and thickness $g = 20$ nm is inserted into the lower Topas layer at $d = 10$ nm beneath the graphene. Gate voltage V_g is applied to the graphene-Topas spacer-polysilicon parallel plate capacitor to control the conductivity of graphene via electrostatic doping effect, as illustrated in Fig. 1(a). Since the polysilicon is very thin and has a moderate relative permittivity, it has little effect on the mode propagation and confinement properties of the hybrid plasmonic waveguide. In addition, it is worth mentioning that the graphene-based hybrid plasmonic waveguide can be produced through state-of-the-art nanoimprint lithography and graphene synthesis and transfer techniques [41–44].

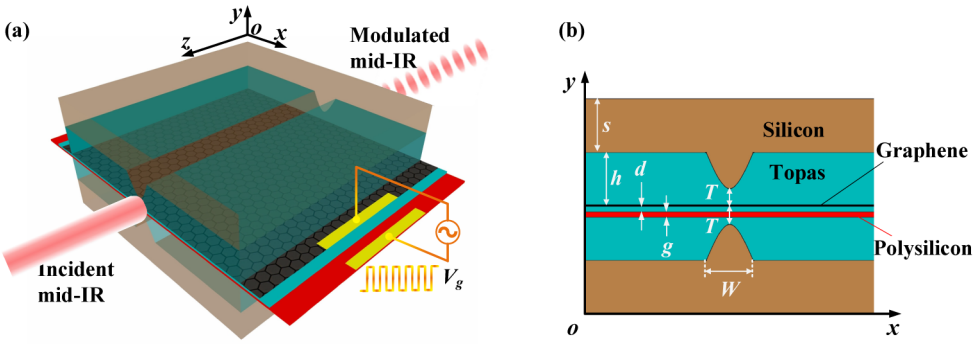

Fig. 1. A graphene-based hybrid plasmonic waveguide. (a) Three-dimensional schematic illustration of the waveguide, where a graphene sheet is embedded between two inner Topas buffer layers and two outer silicon substrate with parabolic ridges, as well as a polysilicon layer is inserted into the lower buffer layer below the graphene acting as a gating layer. (b) Cross-section of the waveguide, where the initial geometric parameters of the waveguide are set as $s = 600$ nm, $h = 600$ nm, $g = 20$ nm, $d = 10$ nm, $T = 50$ nm, and $W = 600$ nm.

In this study, we use the commercial software COMSOL Multiphysics based on the finite element method (FEM) to numerically calculate and analyze the properties of the proposed graphene-based hybrid plasmonic waveguides. Since graphene is actually one-atom-thick 2D material with the excited carriers transporting in its 2D plane, only its in-plane conductivity can be tuned by chemical potential via the electrostatic doping. Modeling graphene layer as a 3D effective isotropic permittivity medium with the effective thickness may lead to overestimation of light absorption at the so-called epsilon-near-zero point [45]. Although modeling the graphene as a 3D effective anisotropic permittivity medium with conductivity dependent in-plane permittivity and constant out-of-plane permittivity is more accurate, it still suffers from larger mesh number and lower computational efficiency in simulation. It has been widely demonstrated that graphene can be effectively treated as a 2D surface conductivity σ_g (or 2D surface impedance $Z_g = 1/\sigma_g$) without thickness ($t_g = 0$) in various

Optics EXPRESS

graphene-based device simulations [23, 40, 45–47]. Therefore, in this study, we model the graphene as a 2D surface conductivity in the related simulation. In the terahertz and mid-IR regions, the surface conductivity for a single-layer of graphene is calculated by the Kubo formula with the intraband and interband contributions [48, 49], as follows,

$$\sigma_g(\omega,\mu_c,\Gamma,T_0)=\sigma_{intra}(\omega,\mu_c,\Gamma,T_0)+\sigma_{inter}(\omega,\mu_c,\Gamma,T_0), \tag{1}$$

$$\sigma_{intra}(\omega,\mu_c,\Gamma,T_0)=\frac{je^2}{\pi\hbar^2(\omega-j2\Gamma)}\int_0^\infty\left(\frac{\partial f_d(\xi,\mu_c,T_0)}{\partial\xi}-\frac{\partial f_d(-\xi,\mu_c,T_0)}{\partial\xi}\right)\xi d\xi, \tag{2}$$

$$\sigma_{inter}(\omega,\mu_c,\Gamma,T_0)=\frac{-je^2(\omega-j2\Gamma)}{\pi\hbar^2}\int_0^\infty\frac{f_d(-\xi,\mu_c,T_0)-f_d(\xi,\mu_c,T_0)}{(\omega-j2\Gamma)^2-4\xi/\hbar^2}d\xi, \tag{3}$$

where ω is the angular frequency, μ_c is the chemical potential or Fermi level, T_0 is the temperature, Γ is the scattering rate with $\Gamma = 2\tau^{-1}$, the relaxation time $\tau = \mu_e\mu_c/(ev_F^2)$, μ_e is the electron mobility, v_F is the Femi velocity, e is the electron charge, ξ is energy, $\hbar$ is the reduced Plank constant, k_B is the Boltzmann constant, and the Fermi-Dirac distribution $f_d(\xi,\mu_c,T)=\left(e^{(\xi-\mu_c)/k_BT}+1\right)^{-1}$. In this study, we assume the temperature T_0 = 300 K and the relaxation time of graphene τ = 1.2 ps, which is estimated from the experimentally available graphene carrier mobility [40,50–52]. It also has been theoretically and experimentally demonstrated that μ_c can be easily tuned from –1.0 to 1.0 eV via the gating structures [49, 53, 54], such as the one shown in Fig. 1, leading to flexibly control the conductivity properties of graphene.

To quantify the characteristics of the proposed graphene-based hybrid plasmonic waveguides, we define the effective index N_{eff}, the propagation length L_{spp}, the figure of merit FOM, and the normalized mode area A [10], as follows,

$$N_{\text{eff}}=k/k_0, \tag{4}$$

$$L_{\text{spp}}=\lambda_0/4\pi\,\text{Im}(N_{\text{eff}}), \tag{5}$$

$$\text{FOM}=\text{Re}(N_{\text{eff}})/\text{Im}(N_{\text{eff}}), \tag{6}$$

$$A=\frac{A_{\text{m}}}{A_0}=\frac{1}{A_0}\frac{\int_{-\infty}^{\infty}W(x,y)\,dxdy}{\max\left[W(x,y)\right]}, \tag{7}$$

$$W(x,y)=\frac{1}{2}\text{Re}\left\{\frac{d[\omega\varepsilon_0\varepsilon_r(x,y)]}{d\omega}\right\}|E(x,y)|^2+\frac{1}{2}\mu_0|H(x,y)|^2, \tag{8}$$

where the propagation constant $k = \beta + i\alpha$, β is the phase constant, and α is the attenuation constant, Re(N_{eff}) and Im(N_{eff}) are the real and imaginary parts of N_{eff}, A_m is the effective mode area, $W(x, y)$ is the energy density of the waveguide; k_0, λ_0, and $A_0 = \lambda_0^2/4$ are the propagation constant, the wavelength, and the diffraction limited mode area in free space, respectively.

3. Results and discussion

Before discussing the propagation and modulation characteristics, we first analyze the surface conductivity and loss tangent of graphene at mid-IR frequencies. According to the Kubo formulas (1)-(3), the real part Re(σ_g) and imaginary-part Im(σ_g) of surface conductivity σ_g, as well as the corresponding loss tangent $tan\ \delta$ = |Re(σ_g)/Im(σ_g)| of graphene as a function of

Optics EXPRESS

chemical potential μ_c at f = 10, 15 and 20 THz are shown in Fig. 2(a). It is found that Re(σ_g) is positive with the value quite near zero (~10^{-2} mS), Im(σ_g) is negative with bigger absolute value, and *tan δ* decreases rapidly at first and then increases very slowly as $|\mu_c|$ increases. Therefore, the graphene layer can be regarded as an effective ultra-thin metal layer capable of supporting SPPs. As the μ_c varies from 0 eV to 1.0 eV, *tan δ* value variation of ~100 times is obtained, implying huge potential capability in achieving good SPP modulation. Likewise, Re(σ_g), Im(σ_g), and *tan δ* as a function of mid-IR frequency f with μ_c = 0.1, 0.6 and 1.0 eV are also present in Fig. 2(b). It is also observed that Re(σ_g) is positive and Im(σ_g) is negative in the frequency band ranging from 10 THz to 20 THz under different μ_c. The *tan δ* values for both μ_c = 0.6 eV and 1.0 eV decrease gradually from 0.013 to 0.007, while the values for μ_c = 0.1 eV rapidly increase from 0.025 to 0.085, as f increasing from 10 THz to 20 THz.

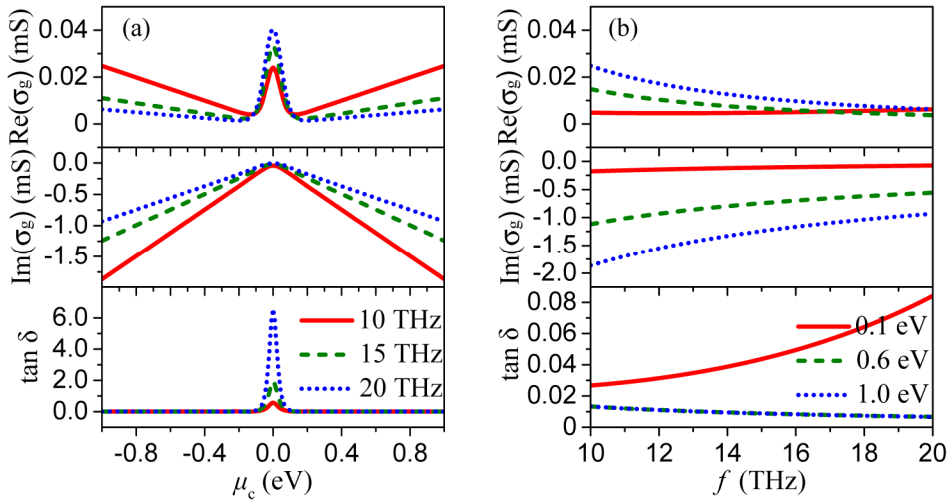

Fig. 2. Dependence of the graphene surface conductivity Re(σ_g), Im(σ_g), and loss tangent *tan δ* on the chemical potential μ_c and frequency f. (a) Re(σ_g), Im(σ_g) and *tan δ* as functions of μ_c with the fixed f = 10, 15, 20 THz. (b) Re(σ_g), Im(σ_g) and *tan δ* as functions of f with the fixed μ_c = 0.1, 0.6, and 1.0 eV.

To demonstrate the strong subwavelength confinement of the proposed waveguide, we plot and compare the fundamental SPP mode distributions of the graphene-based plasmonic waveguides with and without the double parabolic ridges under the same geometric parameters presented in section 2. By taking into account the tunability of graphene at different chemical potential values, we plot the simulated fundamental SPP electric field distributions of the waveguide without parabolic ridges in Figs. 3(a) and 3(c), and of the proposed waveguide with parabolic ridges in Figs. 3(b) and 3(d) with μ_c fixed as 1 and 0.1 eV at 15 THz, respectively. Obviously, the electric field distributions of both waveguides are strongly confined particularly near the graphene layer for the waveguide under μ_c = 0.1 eV, which are much tighter than that under μ_c = 1.0 eV. Owing to the efficient coupling effect of the ridges, the significantly increased light-graphene interaction and super SPP field concentration can be observed inside the nanoscale region between the double ridges with respect to the waveguide without ridges. This is very beneficial for obtaining deep subwavelength confinement for the proposed waveguide. Further, Figs. 3(e) and 3(f) show the propagation length L_{spp} and normalized mode area A for the waveguides with and without ridges as the mid-IR frequency varying from 10 THz to 20 THz with μ_c = 0.1 and 1.0 eV. It clearly shows that the normalized mode area of the proposed waveguide can reach ~10^{-4}-10^{-5}, demonstrating more than one-order smaller compared with that of the hybrid plasmonic waveguide without ridges, while the propagation length of both waveguides almost remains the same level. For μ_c = 1.0 eV, the proposed waveguide can also achieve sufficient long

Optics EXPRESS

propagation length of 12.1-16.7 μm. These properties are greatly significant for the broadband mid-IR centralized transmission and miniaturized integration.

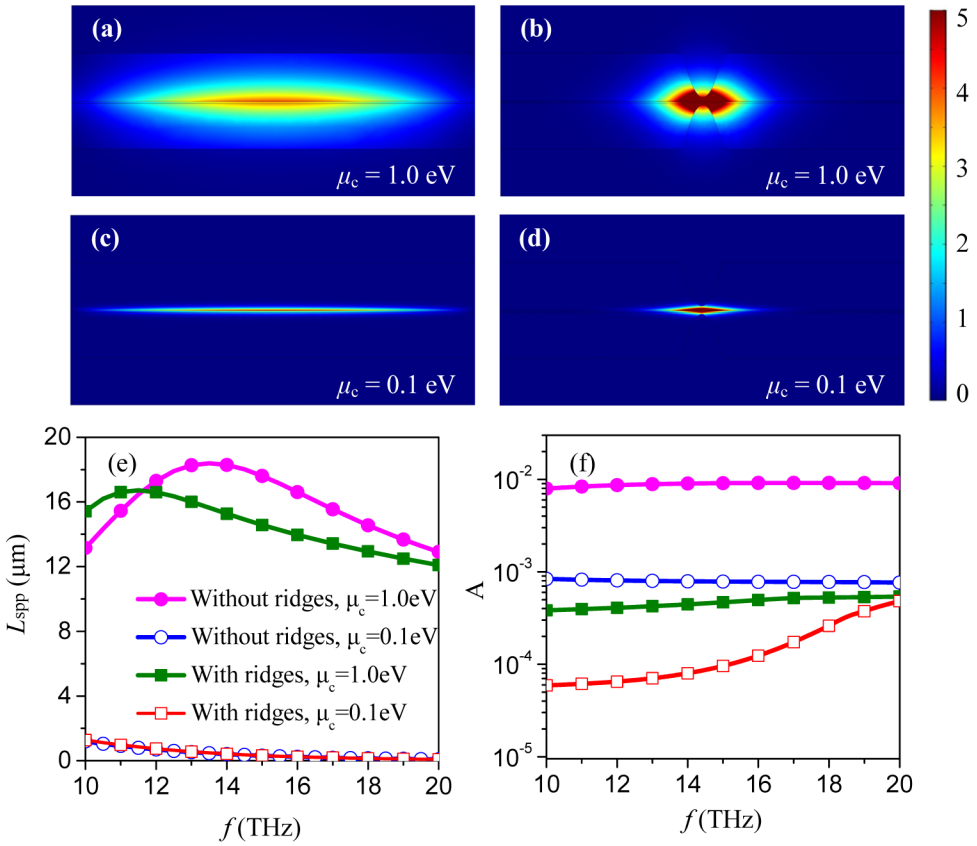

Fig. 3. Comparison of the fundamental SPP mode properties of the hybrid plasmonic waveguides with and without ridges. (a) and (c) are electric field distributions of the waveguide without ridges, and (b) and (d) are electric field distributions of the waveguide with parabolic ridges under the μ_c = 0.1 eV and 1.0 eV at 15 THz, respectively. (e) The propagation length L_{spp} as a function of frequency f. (f) The normalized mode area A as a function of frequency f.

To better understand the propagation properties of the proposed waveguide, the electronic field distributions, the real part effective index Re(N_{eff}), propagation length L_{spp}, and figure of merit FOM between the fundamental (Mode 1) and 4 higher modes (Modes 2-5) are further compared, as shown in Fig. 4. The electric field distributions of the 2-5 modes of the proposed waveguide with μ_c = 1.0 eV at 15 THz are depicted in Figs. 4(a)-4(d), respectively. The dependence of Re(N_{eff}), L_{spp}, and FOM on the frequency f of the waveguide are respectively shown in Figs. 4(e), 4(g), and 4(i) for T = 50 nm, as well as in Figs. 4(g), 4(h), and 4(j) for T = 200 nm while keeping other geometric dimensions the same as that presented in the Fig. 1. The Re(N_{eff}) and FOM of all 5 modes increase as the f increases, implying a stronger field confinement and a higher figure of merit is achieved at higher frequency end. The L_{spp} of first 3 modes will increase to their maximum values and then decrease, while the L_{spp} of first modes 4-5 increases continuously, as the f increases to a higher frequency of 20 THz. Notably, by optimizing the vertex-to-graphene separation T, the Mode 1 can simultaneously achieve larger Re(N_{eff}), L_{spp} and FOM values during the full band 10-20 THz, demonstrating obvious advantages of stronger field confinement, longer propagation length, and better overall optical performance over the rest of higher modes. Therefore, we only

Optics EXPRESS

focus on the fundamental mode properties of the proposed waveguides in the following discussion.

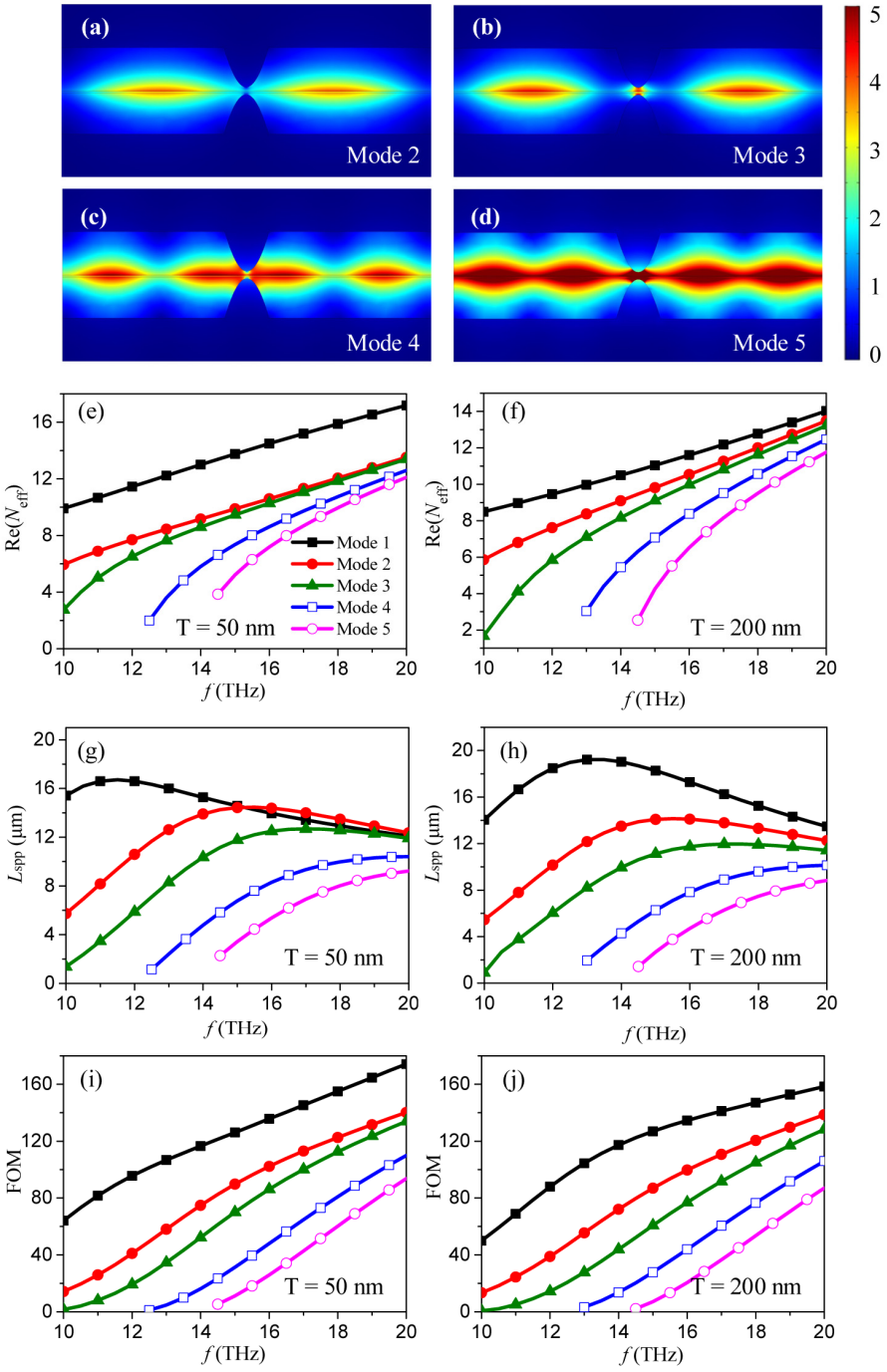

Fig. 4. Electric field distributions, effective indices Re(N_{eff}), propagation length L_{spp} and figure of merit FOM of the proposed waveguide with μ_c = 1 eV. (a)-(d) reveal the electric field distributions of the higher mode 2-5 at 15 THz, respectively. (e)-(f), (g)-(h), and (i)-(j) are Re(N_{eff})~f, L_{spp}~f and FOM~f for T = 50 and 200 nm, respectively, where other geometric parameters are the same as that in Fig. 1.

Optics EXPRESS

Next, we study the effects of the key geometric parameters of the parabolic ridges and the dielectric constants of the buffer materials on the Re(N_{eff}) and L_{spp} for the fundamental mode (Mode 1) of the proposed waveguide. Figures 5(a) and 5(b) depict the Re(N_{eff}) and L_{spp} as functions of the parabolic vertex-to-graphene distance T and the opening width W of the two parabolic ridges with μ_c = 1.0 eV and f = 15 THz, where the parameters are set as W = 600 nm for Fig. 5(a) and T = 50 nm for Fig. 5(b), respectively. It is interesting that the Re(N_{eff}) largely decreases (increases), and the L_{SPP} largely increases (decreases) as T (W) increases. The field distributions, shown in the insets of Fig. 5, clearly demonstrate the tighter SPP confinement can be obtained at smaller T and wider W, which is expected from the larger Re(N_{eff}). To provide some reference for practical applications, the comparison of Re(N_{eff}) and L_{spp} of the proposed waveguides with different buffer layer materials of Al_2O_3, SiO_2 and Topas are presented in Figs. 5(c) and 5(d), where the parameters are assumed as ε_{SiO2} = 3.7 and ε_{Al2O3} = 8 [27], and μ_c = 1 eV. It is clear that the SPP propagation properties also can be flexibly tuned by changing the permittivity of the buffer layer. Because of the lowest permittivity of the Topas, the Re(N_{eff}) (L_{spp}) of the proposed waveguide with Topas buffer layer has the lowest (highest) value with respect to the waveguides with Al_2O_3 and SiO_2 buffer layers.

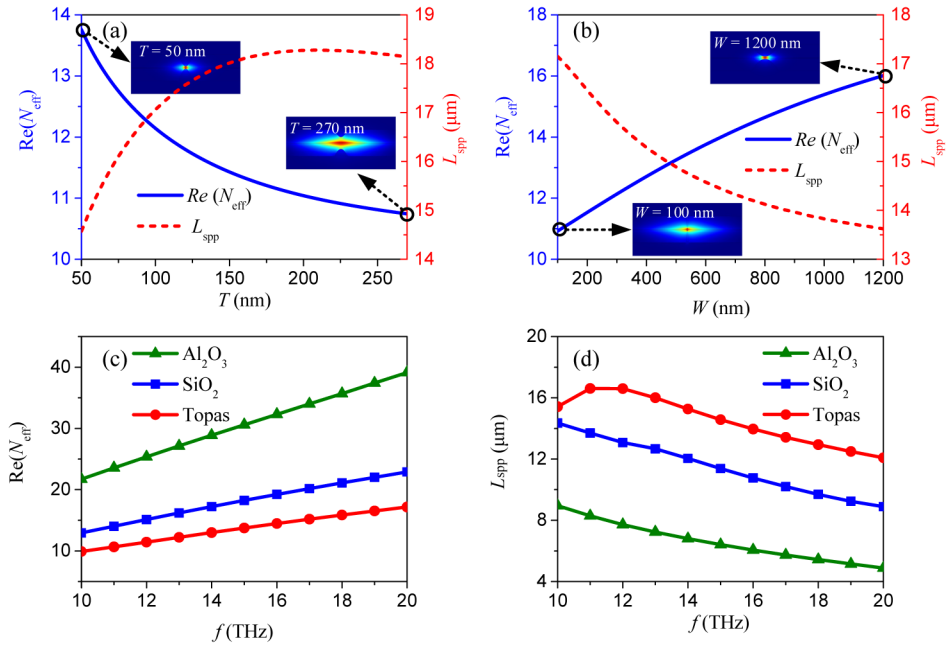

Fig. 5. Dependence of the mode properties on the geometric parameters of the parabolic ridges and the dielectric constants of the buffer materials with μ_c = 1.0 eV. (a) The dependence of Re(N_{eff}) and L_{spp} on T with W = 600 nm at f = 15 THz. (b) The dependence of Re(N_{eff}) and L_{spp} on W with T = 50 nm at f = 15 THz. (c) and (d) present Re(N_{eff}) and L_{spp} as a function of f for the proposed waveguides with different buffer layer materials of Al_2O_3, SiO_2 and Topas, respectively.

Finally, we further demonstrate the broadband modulation performance of fundamental mode for the proposed waveguide. In this hybrid plasmonic waveguide design, the μ_c can be easily controlled by gate voltage V_g, as illustrated in Fig. 1(a). The V_g ~μ_c relation obtained from the formula [49]: $V_g = \frac{e \cdot n_s \cdot d}{\varepsilon_r \varepsilon_0}$, where

Optics EXPRESS

$n_s = \frac{2}{\pi\hbar^2 v_F^2}\int_0^\infty \xi[f_d(\xi,\mu_c,T) - f_d(\xi+2\mu_c,\mu_c,T)]d\xi$, is plotted in Fig. 6(a). It is found that the required value of V_g for achieving the μ_c of 0.1 and 1.0 eV are about 0.38 and 31.33 V, respectively. By taking the advantage of the graphene tunability, the broadband SPP modulation of the proposed absorber can be achieved. As previously shown in Fig. 3, we can clearly see that the SPP propagation characteristics including electric field distributions, propagation length, and normalized mode area can be significantly manipulated by setting different graphene chemical potential μ_c. To further quantitatively evaluate the modulation performance, we calculate the dependence of Re(N_{eff}), attenuation constant α (dB/μm), and transmission t on the μ_c with the frequency fixed at 10, 15, and 20 THz, as respectively shown in Figs. 6(b), 6(c), and 6(d), where t is defined as $10^{-\alpha/10}$, denoting the transmission of the proposed waveguide with 1 μm length. It is observed that both Re(N_{eff}) and α have large values at the beginning with μ_c < 0.1 eV, owing to strong mode confinement and large *tan δ* of the graphene, and both of them continuously decrease with the μ_c increasing when f is fixed. For the center frequency at 15 THz, the α can be actively tuned from 136.9 to 0.3 dB/μm, and the t can be increased from ~0 to ~0.93 as the μ_c increases from 0 to 1.0 eV, demonstrating a huge SPP attenuation tuning capability over 136.6 dB/μm. Owing to the unique parabolic-ridged substrate design, the light-graphene interaction is significantly increased with the electric fields strongly concentrated in graphene layer inside the nanoscale region between the double ridges. Consequently, the change of graphene conductivity plays a major role in the proposed waveguide propagation performance tuning. To the best of our knowledge, the attenuation modulation property of this design is superior to the recently reported broadband waveguide modulators, which have a typical attenuation modulation ranging from 0.1 dB/μm to 5.75 dB/μm [25, 26, 35, 36]. By taking into account the natural doping of graphene from the substrate [25, 55], we set the graphene chemical potential μ_c = 0.1 eV (V_g = 0.38 V) as the "OFF" state point, and μ_c = 1.0 eV (V_g = 31.32 V) as the "ON" state point of the proposed waveguide. Then, the modulation depth is obtained from transmission via $\eta = (t_{ON} - t_{OFF})/t_{ON}$ [33]. To better show the broadband modulation characteristics, the dependence of attenuation α, transmission t, and the modulation depth η on frequency f with the μ_c fixed at 0.1 and 1.0 eV, as respectively shown in Figs. 6(e) and 6(f). It is found that α and t nearly remain constant, 0.28-0.36 dB/μm and 94-92% at ON state, while, both of them vary a lot from 3.39 to 50.94 dB/μm and 45-0% at OFF state when the frequency shifts from 10 to 20 THz. The change of α provides the change of η under different states, which significantly increases with increasing f. In this scenario, the proposed waveguide can achieve a broadband SPP modulation with the modulation depth greater than 51% between 10 and 20 THz, and approach a maximum of 100% at f > 18 THz.

Optics EXPRESS

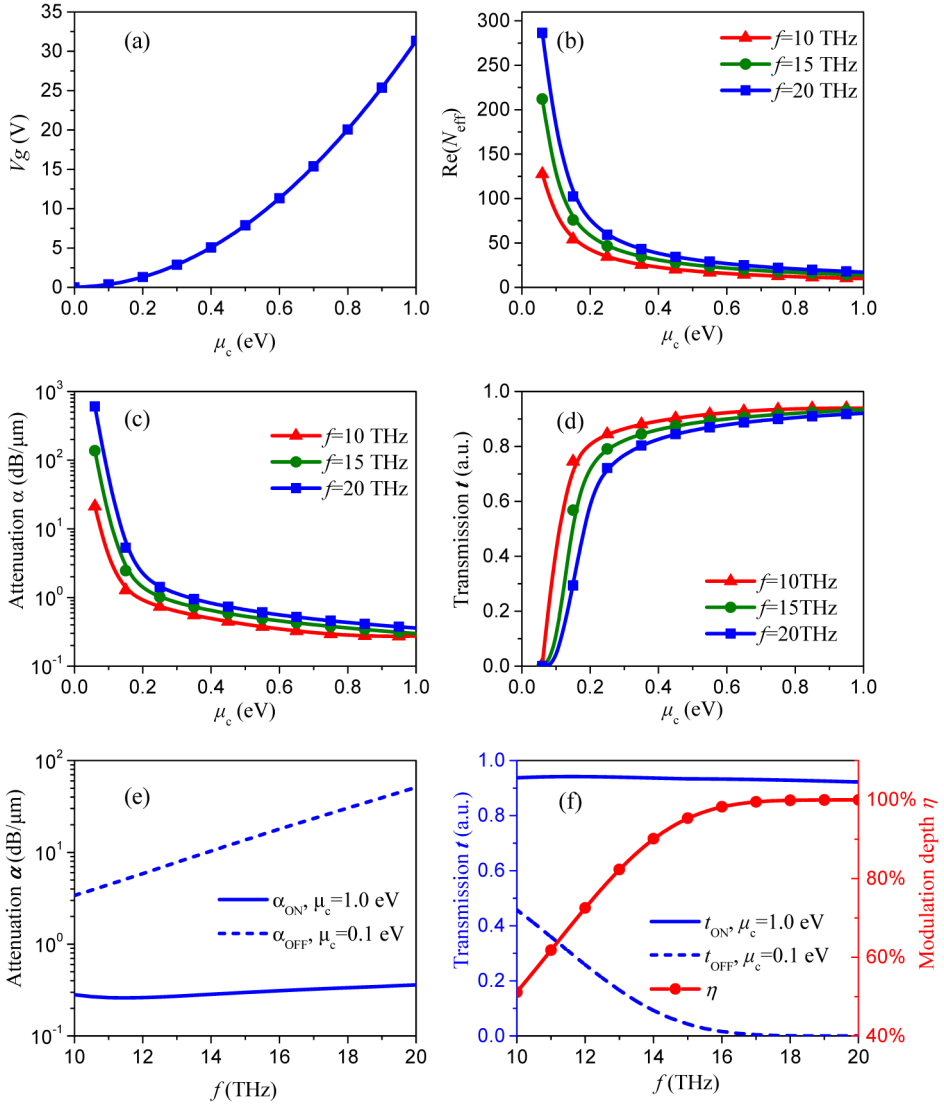

Fig. 6. (a) shows the dependence of chemical potential μ_c on the gate voltage V_g. (b), (c) and (d) depict the dependence of Re(N_{eff}), attenuation α and transmission t on μ_c with the frequency fixed at 10, 15 and 20 THz. (e) and (f) depict the dependence of attenuation α, transmission t and modulation depth η on frequency f with the μ_c fixed at 0.1, 0.6 and 1.0 eV, respectively.

4. Conclusion

In this study, a graphene-based hybrid plasmonic waveguide with double parabolic-ridged silicon substrates have been demonstrated for highly efficient broadband SPP propagation and modulation at mid-IR spectrum. Owing to the unique waveguide structure, significantly enhanced light-graphene interaction and subwavelength SPPs confinement can be achieved. The dependence of propagation properties of the first 5 SPP modes on the key parameters of the parabolic ridges has been studied. The results show that the fundamental SPP mode is superior to other higher SPP modes with longer propagation length (12.1-16.7 μm) and smaller normalized mode area (~10^{-4}) in the mid-IR frequency between 10 THz and 20 THz under the chemical potential of 1.0 eV. Compared with the hybrid plasmonic waveguide without parabolic ridges, the proposed waveguide enables more than one order smaller in the

Optics EXPRESS

normalized mode area with almost the same level of propagation length, which is greatly superior over other conventional metal-based plasmonic waveguides. By tuning the graphene chemical potential from 0.1 eV to 1.0 eV, we have demonstrated broadband modulation of mid-IR guided wave with a modulation depth greater than 51% under the full frequency band of 10-20 THz and a maximum of nearly 100% at $f > 18$ THz. The proposed guiding scheme offers a potential strategy for excellent broadband mid-IR SPP propagation and modulation, which may be flexibly engineered for various high-performance mid-IR and THz devices.

Funding

National Natural Science Foundation of China (61601393); Natural Science Foundation of Fujian Province of China (2016J01321); Natural Science Foundation of Guangdong Province of China (2015A030310009).